Structural Mechanism of Oxidative Regulation of the Phosphatase Cdc25B via an Intramolecular Disulfide Bond[†,‡]

Greg Buhrman,[§] Benjamin Parker,[||] Jungsan Sohn,[||] Johannes Rudolph,*[,||] and Carla Mattos*[,§]

Department of Molecular and Structural Biochemistry, 128 Polk Hall, CB 7622, North Carolina State University, Raleigh, North Carolina 27695, and Department of Biochemistry, LSRC, C125, Mail Stop 3813, Duke University Medical Center, Durham, North Carolina 27710

Received December 6, 2004; Revised Manuscript Received February 9, 2005

ABSTRACT: Cdc25B phosphatase, an important regulator of the cell cycle, forms an intramolecular disulfide bond in response to oxidation leading to reversible inactivation of phosphatase activity. We have obtained a crystallographic time course revealing the structural rearrangements that occur in the P-loop as the enzyme goes from its apo state, through the sulfenic (Cys-SO^-) intermediate, to the stable disulfide. We have also obtained the structures of the irreversibly oxidized sulfinic (Cys-SO_2^-) and sulfonic (Cys-SO_3^-) Cdc25B. The active site P-loop is found in three conformations. In the apoenzyme, the P-loop is in the active conformation. In the sulfenic intermediate, the P-loop partially obstructs the active site cysteine, poised to undergo the conformational changes that accompany disulfide bond formation. In the disulfide form, the P-loop is closed over the active site cysteine, resulting in an enzyme that is unable to bind substrate. The structural changes that occur in the sulfenic intermediate of Cdc25B are distinctly different from those seen in protein tyrosine phosphatase 1B where a five-membered sulfenyl amide ring is generated as the stable end product. This work elucidates the mechanism by which chemistry and structure are coupled in the regulation of Cdc25B by reactive oxygen species.

The Cdc25 phosphatases (Cdc25A, Cdc25B, and Cdc25C in humans) function as essential regulators of cell cycle control during normal eukaryotic cell division and as mediators of the checkpoint response in cells with DNA damage (*1*). These dual-specificity phosphatases (DSPs)[1] belong to a subclass of the protein tyrosine phosphatases (PTPs) and dephosphorylate phospho-Thr14 and phospho-Tyr15 on the Cdk−cyclin complexes (e.g., Cdk2-pTpY−CycA). Dephosphorylation of the Cdk−cyclin complexes leads to activation of these regulatory kinases, phosphorylation of their numerous cellular targets, and cell cycle progression (*2*). The important role of the Cdc25A and Cdc25B homologues in cell cycle regulation is emphasized in the many studies that show their enhanced expression in a wide variety of cancers (*3*). Regulation of the Cdc25 phosphatases is therefore of critical importance in controlling cell proliferation. The activity of the Cdc25 phosphatases is controlled by factors such as intracellular localization, phosphorylation by Cdk−cyclin complexes, degradation, and oxidation by reactive oxygen species (ROS).

It has become increasingly apparent that ROS play a critical role in controlling the activity of a number of PTPs (*4*, *5*), including the Cdc25s (*6*, *7*), and in vivo experiments have shown that they are essential in regulating mitogenic processes (*5*, *8*−*10*). The regulation of the PTPs by ROS is mediated by the one shared feature of this class of enzymes, the P-loop containing the active site sequence CX_5R (Figure 1) (*11*, *12*). The catalytic cysteine in the P-loop in these enzymes sits in a unique dipole environment created by an α-helix (H4 in Figure 1A), the amides of the five X residues, and the conserved arginine (*13*). This conformation generates an unusually low pK_a (5.6−6.3) for the active site cysteine (Cys473 in Cdc25B) (*14*, *15*), making it an optimal nucleophile in the catalytic reaction and also leaving it highly susceptible to oxidation by ROS. Given the instability of the first oxidation of cysteine to sulfenic acid, direct oxidation as a form of reversible regulation is mechanistically feasible only if further oxidation to the sulfinic or sulfonic acids is prevented (*4*). This is accomplished in the phosphatase PTP1B by formation of an unusual sulfenyl−amide bond between the side chain sulfur atom of the active site Cys215 and the backbone amide of the adjacent Ser216 (*16*, *17*). In other families of phosphatases, such as the Cdc25s, there is a nearby cysteine (Cys426 in Cdc25B), the so-called back door cysteine, that forms a disulfide bond with the active site cysteine under mildly oxidative conditions (*7*, *18*, *19*). We have recently demonstrated the transient formation of a sulfenic acid followed by stable formation of a reversible intramolecular disulfide for Cdc25B using kinetic measurements and mass spectrometry (*6*). Herein, we show the structural changes that occur in the P-loop during this

[†] Support for this work was provided by the National Science Foundation (Grant MCB 0237297 to C.M.).

[‡] The coordinates and structure factors for the apo, disulfide, sulfenic, sulfinic, and sulfonic forms of Cdc25B have been deposited in the Protein Data Bank (entries 1YMK, 1YSO, 1YML, 1YM9, and 1YMD, respectively).

* To whom correspondence should be addressed. Phone: (919) 513-2556. Fax: (919) 513-2047. E-mail: carla_mattos@ncsu.edu.

[§] North Carolina State University.

[||] Duke University Medical Center.

[1] Abbreviations: DSP, dual-specificity phosphatase; PTP, protein tyrosine phosphatase; ROS, reactive oxygen species; DTT, dithiothreitol.

10.1021/bi047449f CCC: $30.25
Published on Web 03/17/2005

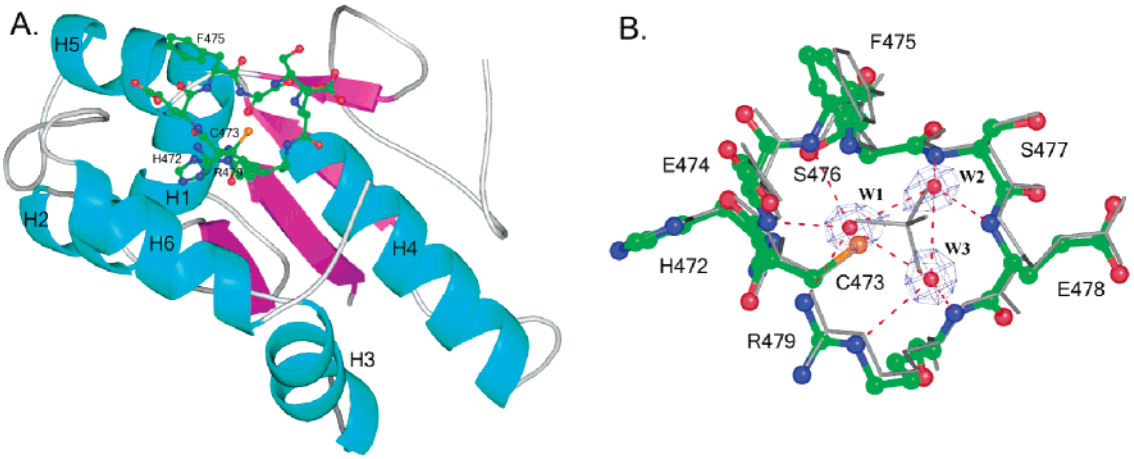

FIGURE 1: Active site P-loop containing residues 472−479 of apo-Cdc25B. (A) Ribbon diagram of the catalytic domain of Cdc25B with the P-loop shown in the ball-and-stick representation. The following color code is used: green for carbon, red for oxygen, blue for nitrogen, and orange for sulfur. (B) Close-up of the P-loop showing the amide ring around the active site Cys473 and the three active site water molecules (represented by red spheres and labeled W1−W3 as described in the text). The electron density for the water molecules is taken from a $2F_o - F_c$ electron density map contoured at the 1.8σ level. The sulfate-bound structure of the P-loop (PDB entry 1QB0) is shown in gray superimposed on the apo structure. Hydrogen bonds are shown as red dashed lines. All least-squares superpositions of structures shown in this and other figures were calculated using LSQMAN (*37*). All figures in this article, with the exception of Figure 4, were generated using the PyMOL Molecular Graphics System (DeLano Scientific, San Carlos, CA).

Table 1: Data Collection and Refinement Statistics

	0 min[a]	20 min[a]	20 min[a]	30 min[a]	80 min[a]
C473 state	reduced	disulfide	Cys-SO_1 sulfenic	Cys-SO_2 sulfinic	Cys-SO_3 sulfonic
space group	$P2_12_12_1$	$P2_12_12_1$	$P2_12_12_1$	$P2_12_12_1$	$P2_12_12_1$
unit cell	$a = 50.23$ Å	$a = 50.20$ Å	$a = 49.86$ Å	$a = 49.27$ Å	$a = 49.70$ Å
	$b = 70.99$ Å	$b = 71.16$ Å	$b = 71.08$ Å	$b = 70.63$ Å	$b = 71.15$ Å
	$c = 73.90$ Å	$c = 73.69$ Å	$c = 74.30$ Å	$c = 73.76$ Å	$c = 74.43$ Å
	$\alpha = \beta = \gamma = 90°$	$\alpha = \beta = \gamma = 90°$	$\alpha = \beta = \gamma = 90°$	$\alpha = \beta = \gamma = 90°$	$\alpha = \beta = \gamma = 90°$
temperature of data collection (K)	100	100	100	100	100
resolution (Å)	1.7	2.0	1.7	2.0	1.7
no. of reflections	29364	17645	29267	16387	28852
redundancy[b]	7.0 (4.5)	6.7 (6.3)	6.9 (4.4)	3.1 (2.8)	7.2 (6.2)
R_{sym} (%)[b,c]	6.7 (17.7)	9.0 (46.9)	7.6 (21.8)	8.0 (40.2)	6.2 (38.0)
completeness (%)	98.6	95.8	98.4	91.1	97.1
average I/σ[b]	28.3 (7.5)	21.6 (4.5)	23.6 (6.5)	13.5 (2.1)	31.2 (3.8)
R_{work}[d]/R_{free}[e] (%)	17.6/19.4	20.8/24.5	18.7/20.7	20.7/23.1	18.6/21.0
rmsd from ideal geometry for bond lengths (Å)	0.009	0.005	0.012	0.013	0.012
rmsd from ideal geometry for bond angles (deg)	1.5	1.3	1.5	1.5	1.5
Ramachandran statistics					
% in favored regions	97	96	96	97	97
% in allowed regions	100	100	100	100	100
no. of protein atoms	1427	1427	1428	1429	1430
no. of water molecules	186	110	171	137	198

[a] Time soaked in 50 μM H_2O_2. [b] The numbers in parentheses describe the relevant value for the highest-resolution shell. [c] $R_{sym} = \sum|I_i - \langle I\rangle|/\sum I$, where I_i is the intensity of the ith term observed and $\langle I\rangle$ is the mean intensity of the reflections. [d] $R_{work} = \sum||F_{obs}| - |F_{calc}||/\sum|F_{obs}|$, where the crystallographic R-factor was calculated using 90% of the reflections against which the model was refined. [e] $R_{free} = \sum||F_{obs}| - |F_{calc}||/\sum|F_{obs}|$, which was calculated using the test set consisting of 10% of the total reflections, randomly selected from the original data set.

process. We have performed a crystallographic time course capturing four different oxidation states of Cys473, providing the first view of how the conformational flexibility of the P-loop leads to the reversible deactivation of a phosphatase as the result of the disulfide bond with the back door cysteine.

EXPERIMENTAL PROCEDURES

Expression, Purification, and Crystallization of the Catalytic Domain of Cdc25B. The catalytic domain of Cdc25B (residues 377−566, herein termed Cdc25B) was expressed and purified as previously described (*15*). The protein was crystallized by modification of a published procedure (*20*). Purified Cdc25B was concentrated to 8.5 mg/mL in 50 mM Tris-HCl (pH 7.5), 50 mM NaCl, 1 mM EDTA, and 1 mM DTT. Crystals were grown using the vapor diffusion method in the presence of a reservoir solution containing 100 mM Tris (pH 7.25), 1.75 M ammonium sulfate, and 1 mM DTT. The initial crystallization drops contained 2 μL of protein solution and 2 μL of reservoir solution. Crystals grew in ~2 weeks. Cdc25B crystallizes with the symmetry of orthorhombic space group $P2_12_12_1$ and with one molecule in the asymmetric unit. The unit cell parameters for each of the five new crystal structures are shown in Table 1.

Data Collection and Model Refinement. Hydrogen peroxide was used as the ROS in our experiments. Before the crystals were soaked in H_2O_2, the crystallization mother liquor was replaced with a buffer solution containing 100 mM Tris-HCl (pH 7.25), 100 mM NaCl, 1 mM DTT, 25%

polyethylene glycol 3350, and 10% glycerol, by extensive buffer exchange. This step was critical for removal of sulfate from the active site of Cdc25B and for providing suitable cryoprotection for data collection at 100 K.

The soaks in the presence of H_2O_2 were carried out by exchanging the buffer used to obtain the apo form with one which differed only in the addition of 50 μM hydrogen peroxide and exclusion of DTT. Crystals were flash-frozen in liquid nitrogen after soaking in the H_2O_2 solution for 20, 30, 70, and 80 min as well as for 6 h, and stored for synchrotron data collection. The crystals soaked in the presence of H_2O_2 for 70 min and 6 h did not diffract well. Data sets were collected at 100 K at the SER-CAT synchrotron beamline (Advance Photon Source, Argonne National Laboratory, Argonne, IL) for crystals flash-frozen after 20, 30, and 80 min soaks in the solution containing H_2O_2. Initial $2F_o - F_c$ and $F_o - F_c$ electron density maps calculated using the published sulfate-bound structure of Cdc25B (*20*) (PDB entry 1QB0) as a starting model (with sulfate and water molecules removed) established that these data sets corresponded to the sulfenic, sulfinic, and sulfonic forms of the protein, respectively.

Having determined that the sulfenic form is present after soaking in the presence of H_2O_2 for 20 min, and that within the next 10 min interval there is irreversible progression to the sulfinic form, we were successful in obtaining the disulfide state by removing the crystals from hydrogen peroxide after a 20 min soak. This was done by buffer exchange back to the conditions used to obtain the apoprotein, but without the DTT. The crystals were flash-frozen after soaking in this H_2O_2-free buffer for 5, 30, 60, 90, and 120 min. X-ray diffraction data were collected for each of these time points at the SER-CAT synchrotron beamline at 100 K. The intramolecular disulfide bond could be seen most clearly using a data set collected after the 90 min back soak. The starting model for refinement against this data set was again the protein model in the sulfate-bound structure (PDB entry 1QB0). The wavelength of the synchrotron X-rays used for data collection was 1 Å in all cases. Data collection and refinement statistics are shown in Table 1.

The program Crystallography and NMR System (CNS) (*21*) was used for all reciprocal space refinement, with a randomly selected 10% of the unique reflections reserved for the calculation of R_{free} (*22*). O (*23*) was used for manual rebuilding of the models with visualization of $F_o - F_c$ and $2F_o - F_c$ electron density maps. A similar protocol was used to refine each of the five models. The initial round of refinement consisted of simulated annealing followed by energy minimization and *B*-factor refinement with CNS. The P-loop was excluded from this initial round of refinement. The protein model was then checked using O and manually adjusted. Subsequent cycles using CNS involved only positional and *B*-factor refinement. The P-loop and water molecules for each model were built using $F_o - F_c$ electron density maps contoured at the 3σ level. CNS topology and parameter files for the oxidized Cys residues were generated with HICCUP (*24*), and initial structures for Cys-SO^-, Cys-SO_2^-, and Cys-SO_3^- were taken from the respective structures of PTP1B (*17*) and moved into the appropriate electron density in the corresponding Cdc25B structures. The structures were checked using MolProbity (*25*).

Substrate Binding Experiments. Cdc25B (1 μM each of untreated wild type, H_2O_2-treated wild type, or C473S mutant) was incubated with 1 μM His_6-Cdk2-pTpY/CycA, and nickel-bead depletion experiments were performed as previously described (*26*). Oxidation of Cdc25B was optimized for generation of the disulfide species (*6*). To show that Cdc25B oxidized to the disulfide does not protect against Cdc25B (WT) dephosphorylation of protein substrate, Cdc25B (untreated WT, H_2O_2-treated WT, or C473S mutant) was incubated with stoichiometric amounts of Cdk2-pTpY/CycA prepared with [γ-^{32}P]ATP as previously described (*27*). Excess (5-fold) Cdc25B (WT) was used to dephosphorylate the unbound protein substrate within 20 s.

RESULTS

Crystals of the catalytic domain of Cdc25B have the symmetry of space group $P2_12_12_1$. They are grown in the presence of high concentrations of ammonium sulfate, and the previously published structure of Cdc25B (PDB entry 1QB0) has a sulfate ion bound in the active site (*20*). The published coordinates were used to phase the five structures presented here: the apo form and four oxidized states. The overall protein structure remained unchanged in all cases, as indicated by a pairwise Cα root-mean-square deviation in the range of 0.10−0.27 Å for the structures with the P-loop residues excluded (473−478). Significant conformational changes were observed only for the P-loop, which is anchored by His472 making H-bonds to the carbonyl of Cys473 and to a nearby water molecule, and by Arg479 through a salt bridge to Glu431.

To capture the oxidized forms of the phosphatase, we first obtained the apo form of the protein by removing the sulfate ion. This was accomplished by transferring the crystals to a buffer containing a mixture of polyethylene glycol and glycerol. The crystal structures of Cdc25B in four oxidation states were obtained by incubating the sulfate-free crystals with 50 μM H_2O_2 for various time intervals. The sulfenic (Cys-SO^-) form was captured by flash-freezing crystals in liquid nitrogen after a 20 min soak in the presence of hydrogen peroxide. Interestingly, accumulation of the sulfenic acid appears to be more favored in the crystals than in solution as this oxidation state is not observed at a significant level using ESI-MS or MALDI-MS detection of intact protein or peptidic fragments (*6*). Even though the disulfide form, with a cross-link between Cys473 and the back door Cys426, is the predominant form under mildly oxidizing conditions in solution, we were unable to capture the disulfide in the crystals without removing H_2O_2. Thus, the disulfide bond was trapped by treating the crystals with 50 μM H_2O_2 for 20 min (to generate the sulfenic form) followed by incubation for 90 min in fresh buffer without H_2O_2 prior to flash-freezing. To obtain the irreversibly oxidized sulfinic (Cys-SO_2^-) and sulfonic (Cys-SO_3^-) forms of Cdc25B, the crystals were incubated for 30 and 80 min, respectively, in a buffer containing 50 μM H_2O_2 prior to being flash-frozen for data collection. Although the rates by which the various oxidized forms are achieved seem to differ in the crystal from those obtained in solution (*6*), our crystallographic studies are in accord with the solution results in that the sulfenic form is transient in nature and leads either to the intramolecular disulfide bond or to higher oxidation states upon exposure to hydrogen peroxide.

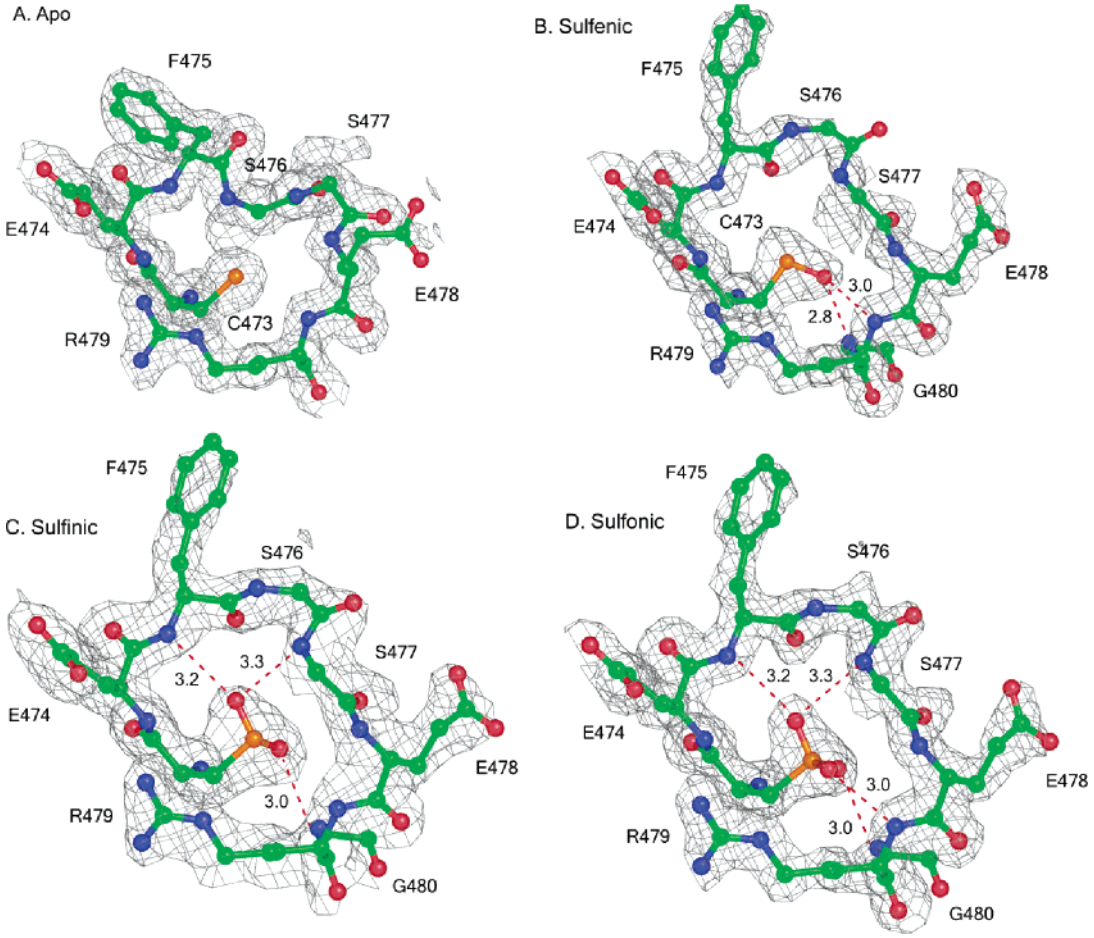

FIGURE 2: Active site P-loop containing residues 472−479 of the apo form and residues 472−480 of the oxygenated form of Cdc25B. (A) Apo-Cdc25B with the active site water molecules omitted. (B) Sulfenic Cdc25B. (C) Sulfinic Cdc25B. (D) Sulfonic Cdc25B. The P-loop is shown using the color code and H-bonding representation of Figure 1. The hydrogen bond distances between the donor and acceptor atoms are given in angstroms. The electron density shown in each panel is from $2F_o - F_c$ electron density maps contoured at the 1.0σ level. The side chains of Ser476 and Ser477 are omitted from the model for clarity. Panels A−D were made with Cdc25B in the same orientation so that differences are due to conformational rearrangements in the P-loop.

Apo Form of Cdc25B. Our crystal structure of the apoenzyme shows no bound sulfate and instead presents three water molecules in the active site (Figure 1B). Each of the three water molecules is 3.0 Å from the other two, and their oxygen atoms form an equilateral triangle at the center of the active site P-loop. The first water molecule (W1) H-bonds to backbone N atoms of Glu474 and Phe475 and with a terminal N atom of the Arg479 side chain that extends from the end of the P-loop back toward Cys473, completing the active site ring of amides. The second water molecule (W2) interacts with the main chain N atoms of Ser477 and Glu478. The third (W3) completes the circle via interactions by H-bonding to the backbone N atom of Arg479 and to Nϵ of the Arg479 side chain. These active site water molecules are located above the reduced Cys473 and mimic the interactions that three of the four sulfate oxygen atoms make with the P-loop residues in the previously published structure (*20*) (Figure 1B). The fourth oxygen atom of the sulfate faces the solvent, and there is no crystallographic water molecule in its place in the apo form. It appears that the sulfate ion is an excellent mimic of the bound substrate, where three of the phosphate oxygen atoms would be held in place for nucleophilic attack by Cys473, with the rest of the substrate binding away from the P-loop. Interestingly, the conformation of the P-loop in the apo form is unchanged relative to the sulfate-bound structure, suggesting that the apo form of the enzyme is in a conformation ready to bind the phosphorylated substrate. The incoming phosphate group of the substrate must displace the three well-ordered water molecules, and the release of these molecules would be expected to contribute entropically to the binding event.

Chemistry and Structure Are Coupled in the Sulfenic Intermediate. The sulfenic, sulfinic, and sulfonic forms of Cdc25B all have the same P-loop conformation, but this structure is very different from that of the apo form where Cys473 is reduced (Figure 2A−D). In all three cases, there would be steric clashes between the oxygenated cysteine and the amide nitrogen atoms of Phe475 and Ser476 if the P-loop were to remain in the conformation found in the apo form. To avoid this unfavorable interaction, residues 475−477 of the P-loop move over the oxygenated Cys473, filling part of the entrance to the active site. The Cα atoms of Ser476 and Ser477 move by 3.8 and 2.3 Å, respectively. This dislocates the hydroxyl oxygen atom of Ser476 by 7.9 Å and its carbonyl oxygen by 4.5 Å. These atoms are replaced by water molecules in the structure of the sulfenic form of the phosphatase. Ser477 moves toward the oxygenated Cys473 (the side chains of Ser476 and Ser477 are not shown in the figure for clarity), and Phe475 is rotated away from the pocket by ~100° on the χ_1 dihedral angle. In this

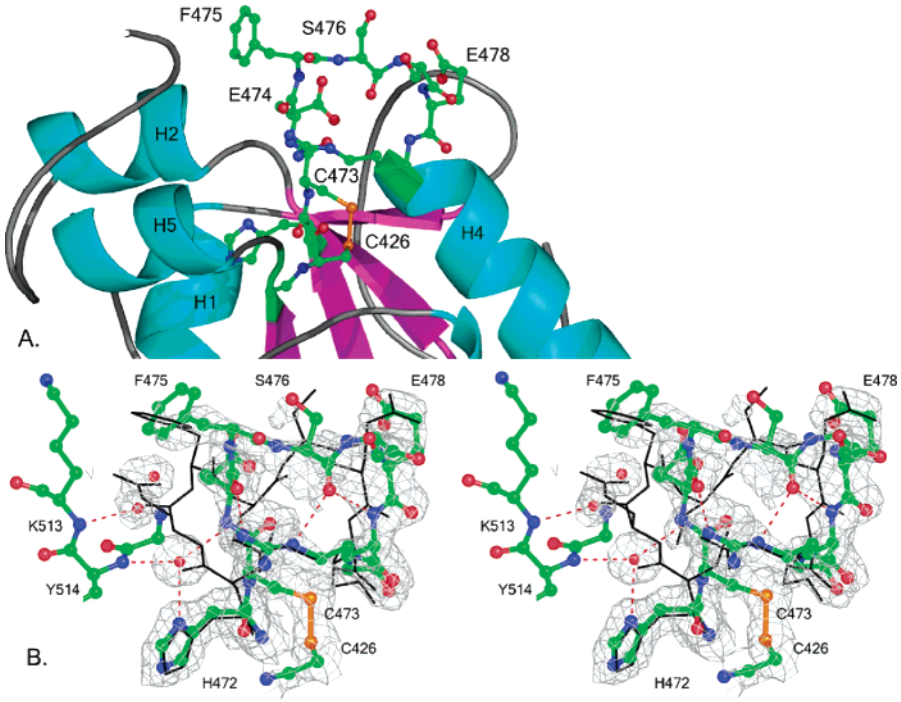

FIGURE 3: Active site P-loop in the disulfide form of Cdc25B. (A) The active site P-loop atoms, including the disulfide bond between Cys473 and Cys426, are shown explicitly with the color code used in Figures 1 and 2 and in the context of the surrounding protein represented in the form of a ribbon diagram. (B) Stereoview of active site P-loop residues 472−480 and residue 426 in the disulfide form of Cdc25B. The apo form of the P-loop is superimposed as a black stick. The electron density is taken from a $2F_o - F_c$ map contoured at the 1.0σ level. The ball-and-stick representation in panel B is color-coded as in panel A, and the P-loop is in the same orientations in both panels A and B.

conformation, the backbone amides of Ser476 and Glu478 are no longer directed inward toward the active site, leaving only the amides of Phe475, Ser477, Arg479, and Gly480 available to interact with the oxidized cysteine. The oxygenated forms of Cys473 reach into the pocket differently than would be expected for substrate. As a result, the oxidized cysteine interacts with the amide of Gly480, rather than with the amide of Glu478. In the sulfenic form, the oxygen atom is facing the end part of the P-loop and H-bonds to the backbone amides of Arg479 (3.0 Å) and Gly480 (2.8 Å) (Figure 2B). This leaves the N-terminal portion of the P-loop without an anchor to the negatively charged sulfenic acid, resulting in higher disorder in this region. Residues 475−478 have higher thermal factors than other residues in the P-loop; there are breaks in the electron density for the backbone atoms of Ser476 and Ser477, and there is no electron density for the side chain atoms of Ser476 (Figure 2B). As discussed below, the crystal structure suggests that the conformation of the P-loop in the sulfenic intermediate, coupled to an increase in disorder, facilitates the formation of the disulfide bond and the resulting conformational change in the active site. In contrast, in the sulfinic and sulfonic forms, both ends of the P-loop are well anchored to the oxygenated active site cysteine. The sulfinic acid interacts with the amides of Phe475 (3.2 Å), Ser477 (3.3 Å), and Gly480 (3.0 Å) (Figure 2C), whereas the sulfonic acid makes all four possible H-bonds with amides of Phe475 (3.2 Å), Ser477 (3.3 Å), Arg479 (3.0 Å), and Gly480 (3.0 Å) (Figure 2D). Not surprisingly, there is an increase in the quality of the electron density for the P-loop, particularly residues 476 and 477, in the more oxygenated forms of Cdc25B.

The Disulfide Bond Sequesters the Active Site Cysteine and Prevents Binding to the Substrate. The P-loop in the disulfide form of Cdc25B collapses toward Arg479 very much like a lid closing over the active site cysteine (Figure 3). To form the disulfide bond, Cys473 moves toward the back door Cys426, pulling the initial part of the P-loop with it and changing the direction of the main chain. As a result, the P-loop residues undergo a dramatic flip with Cα displacements relative to the apo form of 3.5, 4.2, 6.3, and 6.9 Å for Glu474, Phe475, Ser476, and Ser477, respectively. This rearrangement leads to the displacement of functional groups on the side chains of Glu474, Ser476, and Ser477 by as much as 9.8 Å. The unusual conformation of the P-loop in the apo form, with all the amides pointing inward and carbonyl groups directed outward, is converted to one in which some of the backbone carbonyl groups are turned inward. The carbonyl oxygen atom of Ser476 now occupies the center of the distorted P-loop and hydrogen bonds to the amide N atom of Arg479 and to the Nϵ atom of its side chain, replacing one of the three water molecules found at the center of the amide ring in the apo form. In the structure of the disulfide form of Cdc25B, three water molecules are found near Tyr514 and Lys513 in the position occupied by the P-loop in the apo structure (Figure 3B). These water molecules stretch from the collapsed P-loop to a part of the protein that helps anchor the P-loop in the active apo form. The model of the P-loop in the disulfide form is supported by clear electron density for the disulfide bond between Cys473 and Cys426, for residues Cys473, Glu474, Glu478, and Arg479, as well as for the main chain atoms of Phe475, Ser476, and Ser477. There is a break in the electron density between the N and Cα atoms of Phe475, partial electron density for the Phe475 side chain, and no electron density for the side chain Cβ and Oγ atoms of either Ser476 or Ser477. The temperature factors for Phe475, Ser476, and

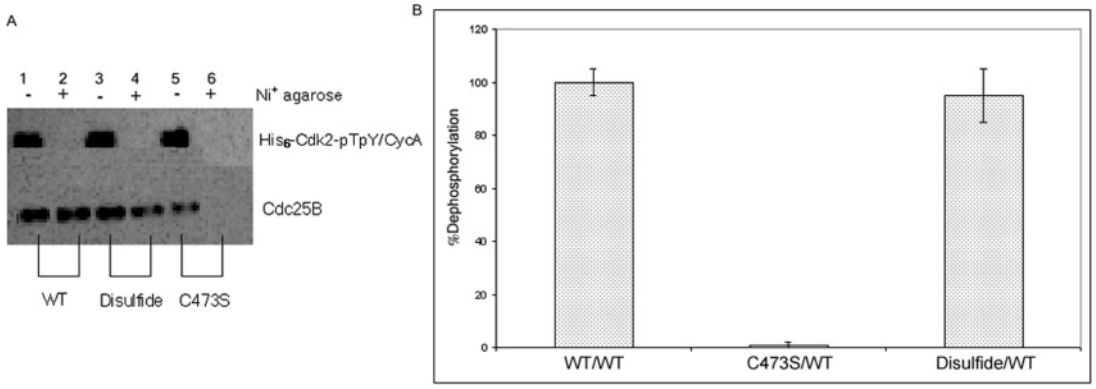

FIGURE 4: Cdc25B binding experiments with the substrate Cdk2-pTpY−CycA complex. (A) SDS−PAGE showing the results for the nickel-bead pull-down experiments. Lanes 1 and 2 contained stoichiometric amounts of wild-type Cdc25B and its substrate in the absence and presence of Ni^+−agarose beads, respectively. In lane 2 there is no Cdk2, which is His-tagged and therefore removed from solution as it binds to the beads. The Cdc25B is not pulled down with the beads, since it releases the substrate after dephosphorylation. Lanes 3 and 4 show the analogous results for Cdc25B under conditions where the intramolecular disulfide bond is formed. Given that the disulfide form has no phosphatase activity, we conclude from lane 4 that it does not bind the substrate, as it is still present in solution after the Ni^+−agarose pull-down assay. Lanes 5 and 6 show the results obtained using the C473S mutant of Cdc25B. Lane 6 shows that all of the mutant Cdc25B is depleted from solution. It is pulled down with the Ni^+-bound substrate, since the dephosphorylation reaction does not occur. (B) Histogram showing the extent of dephosphorylation of the substrate by active wild-type Cdc25B after preincubation of the Cdk2-pTpY−CycA complex with active phosphatase (WT), with the C473S mutant (C473S), or with the protein in the disulfide state generated in the presence of H_2O_2 (Disulfide). The mutant Cdc25B traps the substrate, preventing dephosphorylation, while the disulfide form leaves the substrate available to interact with the active phosphatase.

Ser477 are quite high, suggesting a fair amount of local motion in this area of the structure. Thus, in the disulfide conformation, the two ends of the P-loop are firmly anchored by surrounding residues in the protein, with the three residues at the top of the lid over the active site cysteine appearing to be somewhat more mobile. The main chain atoms of Glu474 and Phe475 in this structure occupy the space where the sulfate ion is found in the sulfate-bound Cdc25B structure, making some of the same interactions with Arg479. This is also the position occupied by the cysteine−phosphate intermediate (*28*) and bound substrate (*29*) in other phosphatase structures. Our crystal structure predicts that the disulfide state of Cdc25B is unable to bind the substrate without a significant conformational rearrangement that can occur only by breaking of the disulfide bond.

It is indeed the case that the disulfide form of Cdc25B does not interact with its substrate Cdk2-pTpY−CycA complex. In nickel-bead pull-down experiments with stoichiometric ratios of the disulfide form of Cdc25B and His-tagged Cdk2 in the Cdk2-pTpY−CycA complex, we were unable to observe a high-affinity complex, as indicated by the fact that the phosphatase is not pulled out of solution by the substrate attached to the Ni^+−agarose beads (Figure 4A). In contrast, when the same experiment is repeated in the presence of the catalytically incompetent C473S mutant, the complex does form as indicated by codepletion of the mutant Cdc25B with substrate in the nickel pull-down experiment. Our conclusion that the disulfide form of Cdc25B does not bind substrate was further supported by the fact that preincubation of a 1:1 ratio of the Cdk2-pTpY−CycA complex and the C473S mutant of Cdc25B protects the substrate against subsequent dephosphorylation by addition of wild-type Cdc25B, whereas incubation of substrate with the disulfide form does not provide any protection (Figure 4B). Taken together, these results establish that C473S is a substrate trapping mutant of Cdc25B and that the disulfide form does not bind the substrate.

DISCUSSION

Mechanism of Reversible Inactivation in Cdc25B. Solution studies have shown that the sulfenic acid is an obligate intermediate in the formation of the intramolecular disulfide bond during reversible regulation of Cdc25B by ROS, and that in the absence of the back door Cys426 the unstable sulfenic acid rapidly oxidizes further to an irreversibly oxygenated form (*6*). Here we complement the kinetic experiments with a view of the structural rearrangements that occur in each oxidation step. The manner in which Cys-SO^- interacts with the P-loop is of critical importance in facilitating the conformational changes necessary to form the intramolecular disulfide bond in Cdc25B. In this intermediate, the section of the P-loop adjacent to the active site cysteine is released from H-bonding interactions observed in the apo form, as it moves toward the closed conformation to avoid steric contacts with the oxygenated cysteine. These changes most likely facilitate the motions that result in the approach of Cys473 toward the back door Cys426. Concurrently, the H-bonding interactions between the O atom of Cys-SO^- and the amide groups on the far side of the P-loop increase the electrophilic character of the oxygenated sulfur atom, thereby making it more prone to nucleophilic attack by the back door cysteine. Once the disulfide bond is made, the active site becomes inaccessible and the protein remains inactive until the disulfide bond is reduced. The superimposed structures of the P-loop in the apo, sulfenic, and disulfide forms show the growing obstruction of the active site cysteine as it reacts to form the disulfide bond (Figure 5). Interestingly, while the P-loops in the sulfinic and sulfonic forms have the intermediate conformation observed for the sulfenic Cdc25B, they do not display the same level of conformational freedom near Cys473. It is significant that the sulfenic form of Cdc25B is a structural intermediate in the conformational rearrangements of the P-loop as well as a chemical intermediate in the oxidation reaction. This phosphatase has evolved to exquisitely couple oxidation

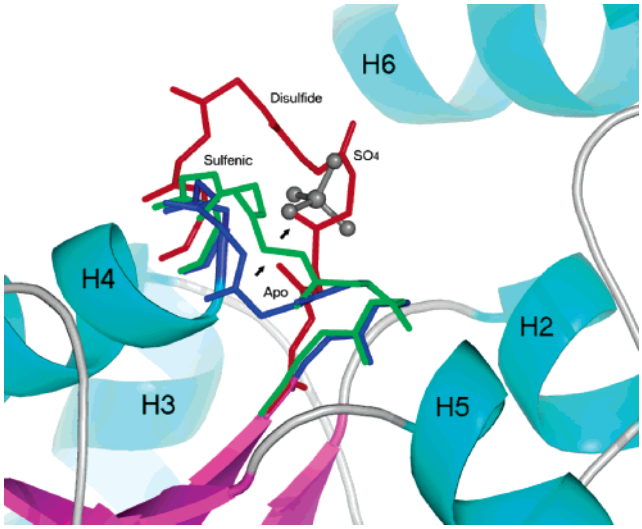

FIGURE 5: Active site P-loop containing residues 472−479 of Cdc25B as it undergoes changes from the reduced to the disulfide form. The main chain atoms of the P-loop are shown in the context of the surrounding protein. The apo form is colored blue, the sulfenic intermediate green, and the disulfide form red. The sulfate taken from the sulfate-bound Cdc25B model (PDB entry 1QB0) is colored gray and indicates the location where the substrate would be expected to bind. Arrows indicate the direction of loop movement that occurs during structural transitions in the reaction from reduced Cys473 to the sulfenic intermediate and finally to the disulfide.

chemistry and the structural rearrangements that lead to its reversible inactivation in the presence of ROS. Disulfide bond formation in transcription factor OxyR in the presence of H_2O_2 is also thought to induce local disorder in the structure, facilitating a conformational change that allows binding to DNA and activation of transcription (*30*). It appears that disorder associated with the sulfenic intermediate in disulfide bond formation is not unique to Cdc25B and may provide a commonly used mechanism through which proteins attain conformational changes in response to ROS.

Comparison with Previously Published Structures of Cdc25. The crystal structure of the apo form of Cdc25A revealed the unique fold of this group of phosphatases and determined structural homology to rhodanese, rather than to other groups of phosphatases (*31*). The salts included in the crystallization solution for Cdc25A were sodium chloride and sodium citrate, neither of which binds in the active site. Thus, the apo form of Cdc25A was obtained. However, no crystallographic water molecules are found in the active site of Cdc25A that are equivalent to the three water molecules present in Cdc25B (Figure 1B). The previously described differences in conformations of the P-loop in Cdc25A and Cdc25B (*20*) lead to the different hydration pattern in the active site. Each of the three crystallographic water molecules that appears in the active site of apo Cdc25B forms a hydrogen bond with a protein atom that is in a different position in Cdc25A. Arg436 and Glu431 in Cdc25A are found in unusual conformations, and the carbonyl group of Ser434 is pointing toward the empty phosphate binding site (*20*, *31*). These residues are the equivalent of Arg479, Glu474, and Ser477 that H-bond with the first, second, and third water molecules, respectively, described above in the Results (Figure 1B). It appears that the deviation of the Cdc25A P-loop from the canonical conformation found in Cdc25B and other PTPases/DSPases disrupts the hydrogen bonding network that would position the active site water molecules observed in our apo structure, as well as the sulfate ion found in the previously determined structure of Cdc25B (*20*).

In the process of determining the crystal structure of Cdc25A, researchers collected several data sets in the presence of heavy atoms for phasing. Electron density maps calculated with a data set taken from crystals grown in 3 mM sodium vanadate clearly showed a disulfide bond between the active site Cys430 and the back door Cys384 (*31*). No bound vanadate was observed in this structure, and the authors did not discuss the conformation of the P-loop. Furthermore, since a model was not pursued using this data set, we cannot compare the structure of the P-loop in the disulfide form of Cdc25A with that of Cdc25B.

Electron density for the disulfide bond between Cys473 and Cys426 in Cdc25B has also been previously reported for a room-temperature crystal structure of Cdc25B (*20*). In this case, the P-loop was not well ordered, but there was some electron density in the active site which the authors interpreted to be a mixture of low-occupancy sulfate ion and solvent molecules. In light of our structure of the disulfide form determined under cryogenic conditions, an alternative possibility is that the electron density in the active site represented the partial occupancy of the P-loop conformation that accompanies the intramolecular disulfide bond (Figure 3). As mentioned in the Results, there is no electron density for the side chains of Ser476 and Ser477 and the *B*-factors in this region are high in our structure of Cdc25B containing the intramolecular disulfide bond. It would not be surprising if there is greater disorder in this region at room temperature, impairing interpretation of the electron density map. This interpretation would be made even more difficult if some fraction of the phosphatase molecules in the crystal had a sulfate in the active site, as Reynolds et al. (*20*) reported to be the case in their structure.

Comparison with PTP1B. Two important groups of topologically distinct phoshatases (*31*) consist of those that have the back door cysteine and those that do not. Cdc25B belongs to the former group and is a good representative of the dual-specificity phosphatases, while PTP1B belongs to the latter group and has been the canonical example for tyrosine phosphatases. The oxidation states of PTP1B, including the sulfenyl amide structure that forms during reversible inactivation, shed light on the process through which one group of phosphatases is reversibly regulated by ROS (*16*, *17*). Here we complement the picture by providing the structural mechanism of reversible inactivation in Cdc25B, a dual-specificity phosphatase that forms the intramolecular disulfide bond. Although inactivation in both groups results in the collapse of the P-loop over the active site Cys residue (Figure 6), the mechanisms by which this happens are intrinsically different. Both groups of enzymes use the sulfenic acid as an intermediate to the more stable reversibly oxidized form. While in both cases the sulfenic acid interacts with the far side of the P-loop, the P-loop in PTP1B, in contrast to Cdc25B, remains unchanged relative to its structure in the apoenzyme (*17*). This is consistent with a mechanism in which Cys215 reacts locally with the amide group of its neighbor Ser216 and is possible due to the presence of the Oγ atom of Ser222 which interacts with Cys-SO^- deep in the active site pocket. Cdc25B has a glycine at

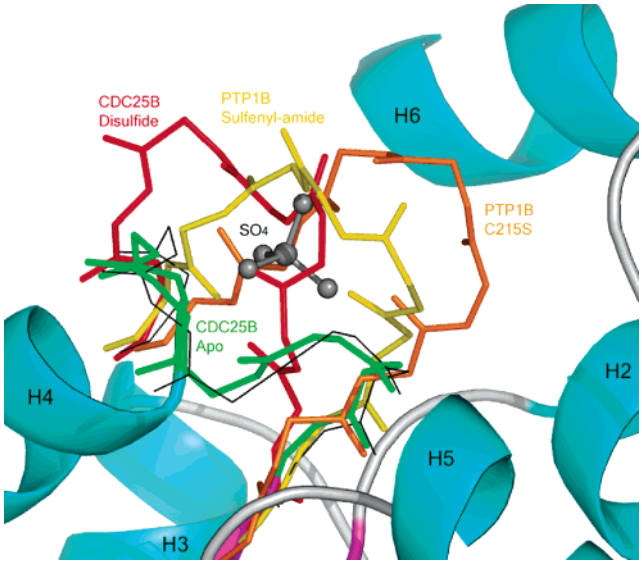

FIGURE 6: Comparison of the P-loop in deactivated forms of Cdc25B and PTP1B. The main chain atoms of the P-loop are shown in the context of the surrounding Cdc25B protein. The orientation of the P-loop in the PTP1B structures relative to Cdc25B was obtained by superposition of the P-loops in the apo forms of the two proteins. Apo-Cdc25B is colored green, and apo-PTP1B (PDB entry 1BZC) is shown as a thin black stick. Residues 472−479 of the disulfide Cdc25B form are colored red. Residues 214−221 of the sulfenyl−amide form of PTP1B (PDB entry 1OEM) are colored yellow and those in the C215S mutant (PDB entry 1I57) orange. The sulfate taken from the sulfate-bound Cdc25B model (PDB entry 1QB0) is colored gray. The surrounding protein represented as a ribbon diagram is from the Cdc25B structure in the apo from.

the analogous position (Gly480). In the absence of the serine side chain, the sulfenic intermediate interacts with the amide group of Gly480 in Cdc25B, forcing the oxygenated cysteine to be located closer to the surface and causing the P-loop to move in the direction of Cys426 to avoid steric hindrance. The conformational differences in the P-loop observed in the sulfenic intermediate during reversible inactivation of Cdc25B versus PTP1B are mechanistically significant and reflect the specific details of each system.

Interestingly, another structure that shows a collapsed P-loop is that of the PTP1B substrate trapping mutant in which the active site Cys215 is changed to a Ser (*32*), analogous to the C473S mutant of Cdc25B discussed above. The C215S PTP1B structure suggests that simply removing the negative charge in the active site is sufficient to cause the collapse of the unusual amide ring structure of the P-loop (Figure 6), yet this mutant has been established to bind substrate (*33*) despite the obstructed active site cysteine observed in the crystal structure. This apparent paradox can be explained by the fact that in the Cys to Ser mutant there is no covalent bond restraining the P-loop to an inactive conformation. As a result, the substrate binding conformation of the P-loop is dynamically accessible and is selected in the presence of a binding partner. The disulfide bond in Cdc25B provides a covalent linkage that holds the P-loop over the active site cysteine such that the amide ring conformation becomes inaccessible. The covalent bond that sequesters the active site Cys215 in the sulfenyl−amide form of PTP1B is expected to have the same effect as the disulfide bond in Cdc25B, disallowing a substrate binding conformation. It appears that in both groups of phosphatases, ROS is

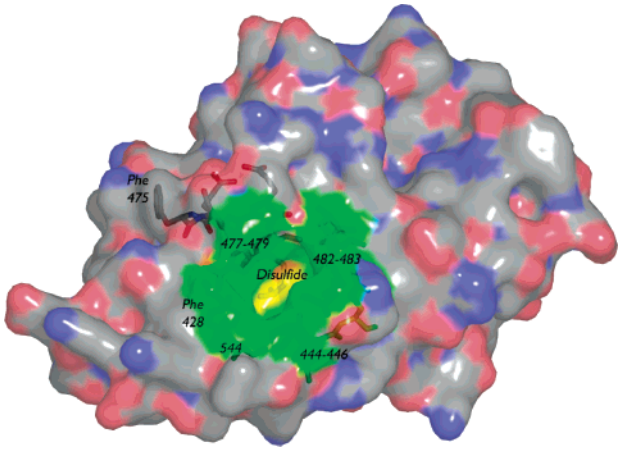

FIGURE 7: Molecular surface of the disulfide form of Cdc25B. In this oxidized form, the P-loop blocks access to the disulfide bond between the active site Cys473 and the back door Cys426, while an adjacent pocket is formed that allows access to the disulfide. Part of the P-loop in this conformation lines part of the wall to this new pocket. Nitrogen atoms are colored blue, oxygen atoms red, and carbon atoms gray. The surface of the pocket is colored green and the disulfide bond yellow. The residues that form the walls of the pocket are drawn explicitly and so are the P-loop residues (with 477−479 and Phe475 labeled).

involved in regulation not only by chemically inactivating the phosphatase but also by stabilizing a structure that cannot bind the substrate. In the case of Cdc25B and probably of related phosphatases containing the back door cysteine, the disulfide bond is buried by the collapsed P-loop, which protects the active site cysteine from either further oxidation or nonspecific reactivation by reducing agents present in the cell.

Solution studies have shown that the disulfide form of Cdc25B is rapidly reduced by thioredoxin but not by glutathione (GSH) (*6*). In contrast, PTP1B (*34*), which forms a sulfenyl−amide structure in the oxidized form, and the LMW phosphatase (*18*), which forms an intramolecular disulfide bond between two cysteine residues in the active site P-loop, are readily reduced by GSH. The sulfenyl−amide structure in PTP1B maintains the active site cysteine in a solvent-exposed conformation that is easily accessed by GSH. A similar situation would be expected for the disulfide bond in the LMW phosphatases. In contrast, the disulfide in Cdc25B is buried at the bottom of the distorted active site, from which GSH is excluded. There is a surface pocket adjacent to the active site lined by many residues, including the back door Cys426 at the base and residues 428, 444−446, 477−479, 482, 483, 544, 547, 549, and 550 forming the walls (Figure 7). This site was identified as the largest pocket in the disulfide state of Cdc25B using CastP, a program that identifies pockets in proteins (*35*). A solvent accessible surface calculation yields a surface area of 161 Å^2 and a volume of 101 Å^3 for this pocket, whereas the corresponding values obtained using a molecular surface calculation are 320 Å^2 and 429 Å^3, respectively. We hypothesize that thioredoxin binds specifically to this pocket to catalyze reduction of the intramolecular disulfide in the Cdc25 dual-specificity phosphatases. This may represent a general reduction mechanism utilized by phosphatases that form a disulfide with a vicinal cysteine located outside the active site P-loop, as is also known to occur in PTEN and KAP (*19*, *36*). Importantly, this structure−function relation-

ship may differentiate between the two main cellular reducing mechanisms (GSH and thioredoxin) found to reactivate PTPs.

CONCLUDING REMARKS

Cdc25B and PTP1B, topologically different proteins, are regulated by ROS through distinct mechanisms that achieve the same results: sequestration of the nucleophilic cysteine and obstruction of the active site. The two groups of phosphatases provide a remarkable example of convergent evolution where similar end results are attained by different processes that reflect the separate structural origins and diverse functional roles. The two distinct mechanisms used in the regulation of phosphatases influence the oxidation/reduction strategies employed by these proteins, result in different responses to cellular oxidation levels, and provide specificity to the cellular reductants used in reactivation. It will be interesting to see how these paradigms of structural changes coupled to chemistry in the reversible inactivation of phosphatases extend to other members of the family and allow for the differential signaling in response to the common ROS second messengers.

ACKNOWLEDGMENT

Data were collected at the Southeast Regional Collaborative Access Team (SER-CAT) 22-ID beamline at the Advance Photon Source. Use of the Advanced Photon Source was supported by the U.S. Department of Energy, Office of Science, Office of Basic Energy Sciences, under Contract W-31-109-Eng-38. We are grateful to the SER-CAT beamline staff for their support.

REFERENCES

1. Strausfeld, U., Labbe, J. C., Fesquet, D., Cavadore, J. C., Picard, A., Sadhu, K., Russell, P., and Doree, M. (1991) Dephosphorylation and activation of a p34cdc2/cyclin B complex in vitro by human CDC25 protein, *Nature 351*, 242−245.
2. Morgan, D. O. (1997) Cyclin-dependent kinases: Engines, clocks, and microprocessors, *Annu. Rev. Cell Dev. Biol. 13*, 261−291.
3. Kristjansdottir, K., and Rudolph, J. (2004) Cdc25 phosphatases and cancer, *Chem. Biol. 11*, 1043−1051.
4. Claiborne, A., Yeh, J. I., Mallett, T. C., Luba, J., Crane, E. J., III, Charrier, V., and Parsonage, D. (1999) Protein-sulfenic acids: Diverse roles for an unlikely player in enzyme catalysis and redox regulation, *Biochemistry 38*, 15407−15416.
5. Finkel, T. (2000) Redox-dependent signal transduction, *FEBS Lett. 476*, 52−54.
6. Sohn, J., and Rudolph, J. (2003) Catalytic and chemical competence of regulation of cdc25 phosphatase by oxidation/reduction, *Biochemistry 42*, 10060−10070.
7. Savitsky, P. A., and Finkel, T. (2002) Redox regulation of Cdc25C, *J. Biol. Chem. 277*, 20535−20540.
8. Rhee, S. G. (1999) Redox signaling: Hydrogen peroxide as intracellular messenger, *Exp. Mol. Med. 31*, 53−59.
9. Devadas, S., Zaritskaya, L., Rhee, S. G., Oberley, L., and Williams, M. S. (2002) Discrete generation of superoxide and hydrogen peroxide by T cell receptor stimulation: Selective regulation of mitogen-activated protein kinase activation and fas ligand expression, *J. Exp. Med. 195*, 59−70.
10. Meng, T. C., Fukada, T., and Tonks, N. K. (2002) Reversible oxidation and inactivation of protein tyrosine phosphatases in vivo, *Mol. Cell 9*, 387−399.
11. Jackson, M. D., and Denu, J. M. (2001) Molecular reactions of protein phosphatases: Insights from structure and chemistry, *Chem. Rev. 101*, 2313−2340.
12. Tonks, N. K., and Neel, B. G. (2001) Combinatorial control of the specificity of protein tyrosine phosphatases, *Curr. Opin. Cell Biol. 13*, 182−195.
13. Peters, G. H., Frimurer, T. M., and Olsen, O. H. (1998) Electrostatic evaluation of the signature motif (H/V)CX5R(S/T) in protein-tyrosine phosphatases, *Biochemistry 37*, 5383−5393.
14. Zhang, Z. Y., and Dixon, J. E. (1993) Active site labeling of the *Yersinia* protein tyrosine phosphatase: The determination of the pK_a of the active site cysteine and the function of the conserved histidine 402, *Biochemistry 32*, 9340−9345.
15. Chen, W., Wilborn, M., and Rudolph, J. (2000) Dual-specific Cdc25B phosphatase: In search of the catalytic acid, *Biochemistry 39*, 10781−10789.
16. Salmeen, A., Andersen, J. N., Myers, M. P., Meng, T. C., Hinks, J. A., Tonks, N. K., and Barford, D. (2003) Redox regulation of protein tyrosine phosphatase 1B involves a sulphenyl-amide intermediate, *Nature 423*, 769−773.
17. van Montfort, R. L., Congreve, M., Tisi, D., Carr, R., and Jhoti, H. (2003) Oxidation state of the active-site cysteine in protein tyrosine phosphatase 1B, *Nature 423*, 773−777.
18. Chiarugi, P., Fiaschi, T., Taddei, M. L., Talini, D., Giannoni, E., Raugei, G., and Ramponi, G. (2001) Two vicinal cysteines confer a peculiar redox regulation to low molecular weight protein tyrosine phosphatase in response to platelet-derived growth factor receptor stimulation, *J. Biol. Chem. 276*, 33478−33487.
19. Lee, S. R., Yang, K. S., Kwon, J., Lee, C., Jeong, W., and Rhee, S. G. (2002) Reversible inactivation of the tumor suppressor PTEN by H_2O_2, *J. Biol. Chem. 277*, 20336−20342.
20. Reynolds, R. A., Yem, A. W., Wolfe, C. L., Deibel, M. R., Jr., Chidester, C. G., and Watenpaugh, K. D. (1999) Crystal structure of the catalytic subunit of Cdc25B required for G2/M phase transition of the cell cycle, *J. Mol. Biol. 293*, 559−568.
21. Brunger, A. T., Adams, P. D., Clore, G. M., Gros, P., Grosse-Kunstleve, R. W., Jiang, J.-S., Kuszewski, J., Nilges, N., Pannu, N. S., Read, R. J., Rice, L. M., Simonson, T., and Warren, G. L. (1998) Crystallographic & NMR system (CNS): A new software system for macromolecular structure determination, *Acta Crystallogr. D54*, 905−921.
22. Brunger, A. T. (1997) Free R Value: Cross-Validation in Crystallography, *Methods Enzymol. 277*, 366−396.
23. Jones, T. A., Zou, J. Y., Cowan, S. W., and Kjeldgaard, M. (1991) Improved methods for building protein models in electron density maps and the location of errors in these models, *Acta Crystallogr. A47*, 110−119.
24. Kleywegt, G. J., and Jones, T. A. (1998) Databases in protein crystallography, *Acta Crystallogr. D54*, 1119−1131.
25. Lovell, S. C., Davis, I. W., Arendall, W. B., III, de Bakker, P. I., Word, J. M., Prisant, M. G., Richardson, J. S., and Richardson, D. C. (2003) Structure validation by Cα geometry: ϕ, ψ and Cβ deviation, *Proteins 50*, 437−450.
26. Rudolph, J. (2002) Catalytic mechanism of Cdc25, *Biochemistry 41*, 14613−14623.
27. Rudolph, J., Epstein, D. M., Parker, L., and Eckstein, J. (2001) Specificity of natural and artificial substrates for human Cdc25A, *Anal. Biochem. 289*, 43−51.
28. Pannifer, A. D., Flint, A. J., Tonks, N. K., and Barford, D. (1998) Visualization of the cysteinyl-phosphate intermediate of a protein-tyrosine phosphatase by X-ray crystallography, *J. Biol. Chem. 273*, 10454−10462.
29. Wang, S., Tabernero, L., Zhang, M., Harms, E., Van Etten, R. L., and Stauffacher, C. V. (2000) Crystal structures of a low-molecular weight protein tyrosine phosphatase from *Saccharomyces cerevisiae* and its complex with the substrate *p*-nitrophenyl phosphate, *Biochemistry 39*, 1903−1914.
30. Lee, C., Lee, S. M., Mukhopadhyay, P., Kim, S. J., Lee, S. C., Ahn, W. S., Yu, M. H., Storz, G., and Ryu, S. E. (2004) Redox regulation of OxyR requires specific disulfide bond formation involving a rapid kinetic reaction path, *Nat. Struct. Mol. Biol. 11*.
31. Fauman, E. B., Cogswell, J. P., Lovejoy, B., Rocque, W. J., Holmes, W., Montana, V. G., Piwnica-Worms, H., Rink, M. J., and Saper, M. A. (1998) Crystal structure of the catalytic domain of the human cell cycle control phosphatase, Cdc25A, *Cell 93*, 617−625.
32. Scapin, G., Patel, S., Patel, V., Kennedy, B., and Asante-Appiah, E. (2001) The structure of apo protein-tyrosine phosphatase 1B C215S mutant: More than just an S → O change, *Protein Sci. 10*, 1596−1605.
33. Zhang, Y. L., Yao, Z. J., Sarmiento, M., Wu, L., Burke, T. R., Jr., and Zhang, Z. Y. (2000) Thermodynamic study of ligand binding to protein-tyrosine phosphatase 1B and its substrate-trapping mutants, *J. Biol. Chem. 275*, 34205−34212.

34. Denu, J. M., and Tanner, K. G. (1998) Specific and reversible inactivation of protein tyrosine phosphatases by hydrogen peroxide: Evidence for a sulfenic acid intermediate and implications for redox regulation, *Biochemistry 37*, 5633−5642.
35. Liang, J., Edelsbrunner, H., and Woodward, C. (1998) Anatomy of protein pockets and cavities: Measurement of binding site geometry and implications for ligand design, *Protein Sci. 7*, 1884−1897.
36. Song, H., Hanlon, N., Brown, N. R., Noble, M. E., Johnson, L. N., and Barford, D. (2001) Phosphoprotein−protein interactions revealed by the crystal structure of kinase-associated phosphatase in complex with phosphoCDK2, *Mol. Cell 7*, 615−626.
37. Kleywegt, G. J., and Jones, T. A. (1994) A super position, *ESF/CCP4 Newsletter 31*, 9−14.

BI047449F